High-frequency conductivity of electrons in double quantum wells under an in-plane magnetic field

1996 J. Phys.: Condens. Matter 8 3003

(http://iopscience.iop.org/0953-8984/8/17/012)

J. Phys.: Condens. Matter **8** (1996) 3003–3017. Printed in the UK

High-frequency conductivity of electrons in double quantum wells under an in-plane magnetic field

O G Balev and F T Vasko

Institute of Semiconductor Physics, National Academy of Sciences, Prospekt Nauki 45, Kiev-28, 252650, Ukraine

Received 8 December 1995

Abstract. The high-frequency response of electrons in double quantum wells (DQWs) under an in-plane magnetic field is considered. The absorption, the Voigt effect and the transverse dipole moment due to electron transitions between tunnel-coupled levels are calculated for excitation by an electric field parallel to the 2D plane; the depolarization field, which is perpendicular to the 2D plane, is also taken into account. Strong modification of the intersubband absorption spectrum (the appearance of two absorption peaks, which demonstrate different collisionless broadening and shift) is found under increasing magnetic field. The spectral dependencies of the Voigt effect and induced dipole moment are calculated. Such dependencies are different in essence for small magnetic fields, for which both tunnel-coupled states are occupied; for intermediate magnetic fields, for which the Fermi level intersects the anticrossing gap; and for large fields, for which the electrons are localized in two valleys of the lowest level. Numerical estimates of these effects are presented for typical DQW structures.

1. Introduction

Electron transport phenomena and optical processes in DQWs have been widely studied in the past (see references in [1, 2]). Peculiarities of such phenomena in DQWs under an in-plane magnetic field $\boldsymbol{H}$ are related to modification of the energy spectra of tunnel-coupled pairs of levels originating from the ground states of left (l-) and right (r-) QWs. Apart from the increase of the level splitting and the shift of the dispersion curve minima of uncoupled QWs in the plane of 2D momentum $\boldsymbol{p}$, an anticrossing of these curves (and, therefore, an additional minimum) appears [3] in sufficiently strong magnetic fields. These modifications of the energy spectrum not only change the magnetotransport phenomena [4–7] and processes under interband optical excitation [8, 9], but also lead to peculiarities in the response to the high-frequency electric field. In conditions where $\hbar\omega$ (ω is the frequency) is smaller than the energies of the next intersubband transitions, such a response is determined by the contribution of the electron transitions between tunnel-coupled levels. The response is substantially affected by the above-mentioned modifications of the electron spectrum, if ω is larger than the typical scattering rate.

In this paper, consideration of the absorption, the Voigt effect, and the *transverse* dipole moment due to electron transitions between tunnel-coupled levels is presented for excitation by an *in-plane* electric field. The spectral dependencies are different for low electron densities—for which only the lowest of the tunnel-coupled levels is occupied—and for high densities—for which with increasing H three different cases are realized: (i) small H, when the electrons populate both levels; (ii) intermediate H, when the Fermi level intersects the

0953-8984/96/173003+15$19.50

anticrossing gap; and (iii) large H, when the electrons are localized in two separate valleys of the lowest level. Under an in-plane magnetic field, intersubband transitions in DQWs are allowed not only for the component of the electric field transverse to the DQW plane, but also for the longitudinal electric field component (such a mechanism has been discussed earlier in connection with intersubband transitions in inversion layers [10]). The broadening of the absorption peaks for such transitions is determined by collisional smearing of these peaks as well as by collisionless broadening caused by the difference between the nonparabolic dispersion laws of the tunnel-coupled states. In addition, due to shifts of the minima from $\boldsymbol{p} = 0$, the square-root singularity of absorption appears in the collisionless approximation at the lower edge of the absorption region (which is independent of H) if the effect of the depolarization is neglected. Transformation of the linearly polarized high-frequency wave to an elliptically polarized wave—the Voigt effect—is possible due to anisotropy of the electron dispersion laws in the 2D plane. In the collisionless approximation, the effect of the depolarization, as we will show, can lead to a strong increase of the Voigt effect, due to virtual intersubband transitions, and to an additional δ-shaped absorption peak at a frequency within the upper region of transparency. It is shown that these resonant effects are more likely to be observed in the DQWs with substantial tunnel coupling and they strongly depend on the value of H (for example, they are absent in case (iii)). One more effect is the appearance of a high-frequency dipole moment across DQWs, which is induced by an in-plane electric field perpendicular to the $\boldsymbol{H}$-direction (the Hall geometry). Such an induced transverse dipole moment can lead to excitation of the waveguide modes that propagate along the DQW plane. In addition, properties of the depolarization field, which appears in the self-consistent description of the response, are modified substantially due to the transverse contribution. Such calculations of the depolarization effect are similar to the scheme developed in [11, 12] (the case of wide parabolic QW [12] is similar to the DQW case, because in both cases the energy spectra are strongly modified under an in-plane magnetic field). As a result of our calculations, expressions for the two-dimensional conductivity and longitudinal–transverse susceptibility are obtained, and the pertinent characteristics of the high-frequency response are determined.

The paper is organized as follows. In section 2 we present basic relations describing the effective response of the system under consideration. The spectral dependencies of the response function and its dependence on the magnetic field and tunnelling matrix element are studied in section 3. The consideration of the absorption, the resonance Voigt effect and the longitudinal–transverse susceptibility is described in section 4. In section 5 we present concluding remarks.

2. Basic relations for the response

Modification of the electron spectra in DQWs under an in-plane magnetic [3] field is described within the basis of the orbitals of the l- and r-QW states (denoted below as ϕ_{lz} and ϕ_{rz}), i.e., using an 'isospin' representation [13]. Assuming that the magnetic field does not change these orbitals and the tunnel matrix element T significantly, we have in such a representation the 2×2 matrix Hamiltonian

$$\hat{h}_{\boldsymbol{p}} = \varepsilon_p + \begin{bmatrix} \Delta(p_y)/2 & T \\ T & -\Delta(p_y)/2 \end{bmatrix}. \tag{1}$$

Here $\varepsilon_p = p^2/2m$, $\boldsymbol{p} = (p_x, p_y)$ is the 2D momentum, and m is the effective mass. In the magnetic field $\boldsymbol{H} \parallel 0X$, the level splitting $\Delta(p_y)$ appears to be dependent on the 2D

momentum as follows:

$$\Delta(p_y) = \Delta - 2v_H p_y + \delta_H \tag{2}$$

where Δ is the level splitting of the ground states in the l- and r-QWs without tunnelling, and the typical velocity $v_H = \omega_c \Delta z/2$ is represented through the cyclotron frequency ω_c and the distance between the centres of the left and right QWs, Δz. The contribution in equation (2) quadratic in H, δ_H, is usually negligible, because $2\delta_H \ll \varepsilon_H$ (here $\varepsilon_H = mv_H^2$ is the energy characterizing the influence of the in-plane magnetic field on the DQW system). Moreover, in the case of a symmetric ($\Delta = 0$) DQW structure, $\delta_H = 0$. According to the Hamiltonian (1) the dispersion laws $\varepsilon_{\pm \boldsymbol{p}}$ and the velocity operator $\hat{\boldsymbol{v}}_{\boldsymbol{p}}$ are anisotropic:

$$\varepsilon_{\pm \boldsymbol{p}} = \varepsilon_p \pm \Delta_T(p_y)/2 \qquad \Delta_T(p_y) = \sqrt{\Delta^2(p_y) + (2T)^2}. \tag{3}$$

In addition, the y-component of $\hat{\boldsymbol{v}}_{\boldsymbol{p}}$ has the matrix addendum given by

$$(\hat{\boldsymbol{v}}_{\boldsymbol{p}})_x = \frac{p_x}{m} \qquad (\hat{\boldsymbol{v}}_{\boldsymbol{p}})_y = \frac{p_y}{m} + \begin{bmatrix} v_H & 0 \\ 0 & -v_H \end{bmatrix}. \tag{4}$$

The above-described peculiarities of the electron dynamics give rise to a possibility of excitation of the intersubband transitions by the y-component of the field, collisionless broadening of the pertinent peaks, and the appearance of a transverse dipole moment.

We begin the calculation of the response of the collisionless quasi-two-dimensional electron system in the DQWs to the in-plane high-frequency external electric field

$$\boldsymbol{E} \exp(-\mathrm{i}\omega t)$$

(the factor $\exp(-\mathrm{i}\omega t)$ is omitted below) by writing the perturbation operator (including the induced depolarization contribution) as

$$\delta\hat{h}_{\boldsymbol{p}} = \frac{\mathrm{i}e}{\omega}\boldsymbol{E} \cdot \hat{\boldsymbol{v}}_{\boldsymbol{p}} + \hat{w}_\omega. \tag{5}$$

The matrix electrostatic potential $\hat{w}_\omega$ appears due to redistribution of the electron charge in the DQWs caused by the external electric field, and is determined from the Poisson equation [11, 14] as

$$(\hat{w}_\omega)_{jj'} = \int \mathrm{d}z\ \phi_{jz} w_z \phi_{j'z} \qquad w_z = -\frac{4\pi e^2}{\epsilon}\int_{-\infty}^{z} \mathrm{d}z'\ (z - z')\,\delta n_{z'} \tag{6}$$

where the dielectric permittivity, ϵ, is taken as uniform across the DQWs. The potential w_z should be calculated on the basis of the orbitals of the l- and r-QWs (in the same way as the components of the matrix Hamiltonian (1) were).

The induced charge density in (6), $e\,\delta n_z$, can be written using the orbitals ϕ_{jz} and the self-consistent nonequilibrium addendum to the density matrix, $\delta\hat{\rho}_{\boldsymbol{p}\omega}$, as

$$e\,\delta n_z = e\sum_{jj'} \delta n_{jj'}\,\phi_{jz}\phi_{j'z} \qquad \delta\hat{n} = \frac{2}{L^2}\sum_{\boldsymbol{p}} \delta\hat{\rho}_{\boldsymbol{p}\omega}. \tag{7}$$

Here $j, j' = \mathrm{l}, \mathrm{r}$, the factor 2 is due to the assumed spin degeneracy, and L^2 is the normalization area. To simplify the notation, we omit argument ω in w_z, δn_z, $\delta\hat{n}$. The self-consistent addendum to the density matrix $\delta\hat{\rho}_{\boldsymbol{p}\omega}$ linearized on the basis of the perturbation (5) can be represented using the equilibrium density matrix, $\hat{\rho}_{eq}$, as

$$\delta\hat{\rho}_{\boldsymbol{p}\omega} = -\frac{\mathrm{i}}{\hbar}\int_{-\infty}^{0} \mathrm{d}\tau\ \mathrm{e}^{(\lambda\tau - \mathrm{i}\omega\tau)}\mathrm{e}^{(\mathrm{i}/\hbar)\hat{h}_p\tau}\left[\frac{\mathrm{i}e}{\omega}\boldsymbol{E} \cdot \hat{\boldsymbol{v}}_{\boldsymbol{p}} + \hat{w}_\omega, \hat{\rho}_{eq}\right]\mathrm{e}^{-(\mathrm{i}/\hbar)\hat{h}_p\tau} \tag{8}$$

where $\lambda \to +0$ in the collisionless case, and it can be replaced by $\Gamma/\hbar$, where phenomenologically introducing the broadening Γ provides the possibility of estimating the smoothing of the spectrum peculiarities due to collisions.

Substituting (8) into (7) and using the relation between the matrices $\hat{w}_\omega$ and $\delta\hat{n}$ (following from (6) and (7)), we express the depolarization contribution in the perturbation, $\hat{w}_\omega$, through the external perturbation. Neglecting the exponentially small overlapping of the orbitals in the expressions given above (only the tunnel contribution in (1) describes a mixing of the states of the l- and r-QWs), we can consider the matrices $\hat{w}_\omega$ and $\delta\hat{n}$ as diagonal. Due to the conservation of the total electron charge in the DQWs, $\mathrm{tr}(\delta\hat{n}) = 0$, the depolarization contribution can be described through the interwell redistribution of the concentration $\Delta n_\omega = \mathrm{tr}(\hat{\sigma}_z\,\delta\hat{n})/2$, according to relation

$$\hat{w}_\omega = (2\pi e^2\,\Delta z/\epsilon)\alpha\,\Delta n_\omega\,\hat{\sigma}_z \tag{9}$$

in which $\hat{\sigma}_z$ is the Pauli matrix, and the trace is taken over the discrete isospin variable. For Δn_ω we have the inhomogeneous equation

$$\Delta n_\omega - \alpha\Pi(\omega)\,\Delta n_\omega = -\mathrm{i}\frac{\epsilon E_y v_H}{2\pi e\,\Delta z\,\omega}\Pi(\omega). \tag{10}$$

Here $\Pi(\omega)$ is the response function, typical for the Kubo formalism. It is given by

$$\Pi(\omega) = -\frac{2\pi\mathrm{i}e^2\,\Delta z}{\hbar\epsilon L^2}\int_{-\infty}^{0}\mathrm{d}\tau\;\mathrm{e}^{(\lambda\tau-\mathrm{i}\omega\tau)}\sum_{\boldsymbol{p}}\mathrm{tr}(\hat{\rho}_{eq}[\mathrm{e}^{-(\mathrm{i}/\hbar)\hat{h}_p\tau}\hat{\sigma}_z\mathrm{e}^{(\mathrm{i}/\hbar)\hat{h}_p\tau},\hat{\sigma}_z]). \tag{11}$$

In (9) and (10) the dimensionless constant of the Coulomb interaction in the DQWs, α, is given as

$$\alpha = \int_{-\infty}^{\infty}\mathrm{d}z\;(\phi_{lz}^2 - \phi_{rz}^2)\int_{-\infty}^{z}\mathrm{d}z'\;(z-z')(\phi_{rz'}^2 - \phi_{lz'}^2)/\Delta z. \tag{12}$$

In the flat-band DQWs, $\alpha \approx 1 - 0.21d/\Delta z$; d is the width of a QW, $\Delta z \approx d + d_b$, and d_b is the barrier width.

The induced current density, $\delta\boldsymbol{J}_\omega$, can be written using (8) as

$$\delta\boldsymbol{J}_\omega = \mathrm{i}\frac{e^2 n}{m\omega}\boldsymbol{E} + \frac{2e}{L^2}\sum_{\boldsymbol{p}}\mathrm{tr}(\hat{\boldsymbol{v}}_{\boldsymbol{p}}\,\delta\hat{\rho}_{\boldsymbol{p}\omega}) \tag{13}$$

where n is the total electron density in DQWs. Due to the redistribution of the electron density discussed above, a transverse dipole moment is induced by the field E_y; this can be expressed as

$$\delta P_\omega = e\int_{-\infty}^{\infty}\mathrm{d}z\;z\,\delta n_z \approx -e\,\Delta z\,\Delta n_\omega \tag{14}$$

and the contribution to δP_ω due to the field E_x is equal to zero according to the absence of a Lorentz force for such geometry. Using the expression for Δn_ω determined by (10)–(12), and introducing the components of the effective conductivity tensor via the relation $\delta\boldsymbol{J}_\omega = \hat{\sigma}(\omega)\boldsymbol{E}$, we have for the diagonal components of the conductivity

$$\sigma_{xx}(\omega) = \mathrm{i}\frac{e^2 n}{m\omega} \qquad \sigma_{yy}(\omega) = \mathrm{i}\frac{e^2 n}{m\omega} + \mathrm{i}\frac{\epsilon v_H^2}{\pi\omega\,\Delta z}\frac{\Pi(\omega)}{1-\alpha\Pi(\omega)} \tag{15}$$

and the nondiagonal components are equal to zero. This property and the absence of the intersubband contribution in σ_{xx} follow from the form of the velocity operator (4).

Analogously, from (14), the dimensionless longitudinal–transverse (i.e., expressing the z-component of the dipole moment as a response to the y-component of the electric field) susceptibility $\chi_\perp(\omega) = \delta P_\omega/(E_y\,\Delta z)$ is obtained as

$$\chi_\perp(\omega) = -\mathrm{i}\frac{\epsilon v_H}{2\pi\omega\,\Delta z}\frac{\Pi(\omega)}{1-\alpha\Pi(\omega)}. \tag{16}$$

Hence we should calculate $\Pi(\omega)$ given by (11) and the kinetic coefficients (15) and (16).

3. The response function

Here we will calculate the response function $\Pi(\omega)$ from (11) in the case of strongly degenerate electrons, using the dispersion law (3), the matrix elements of $\hat{\sigma}_z$, and the calculation of the trace on the basis of the eigenfunctions of (1). Thus we obtain the response function as

$$\Pi(\omega) = \frac{2\pi e^2\,\Delta z}{\epsilon L^2}\sum_{j,j',\boldsymbol{p}}\frac{\Theta(\varepsilon_F-\varepsilon_{j\boldsymbol{p}})-\Theta(\varepsilon_F-\varepsilon_{j'\boldsymbol{p}})}{\varepsilon_{j\boldsymbol{p}}-\varepsilon_{j'\boldsymbol{p}}+\hbar\omega+\mathrm{i}\Gamma}\{[\Delta(p_y)/2T]^2+1\}^{-1} \tag{17}$$

where $\Theta(x)$ is the step function and ε_F is the Fermi energy. The Fermi energy depends on the magnetic field and DQW parameters and must be determined from the conservation law for the total electron concentration:

$$n = \frac{2}{L^2}\sum_{\boldsymbol{p}}\Theta(\varepsilon_F-\varepsilon_{j\boldsymbol{p}}). \tag{18}$$

Neglecting the effect of the depolarization (i.e., formally assuming $\alpha = 0$ in the formulas above), we find that $(\sigma_{yy}-\sigma_{xx})$ and $\chi_\perp$ are proportional to $\Pi(\omega)$. As a result, the absorption, the phase shift in the Voigt effect, and the induced dipole moment are expressed through the response function. In addition, the properties of $\Pi(\omega)$ itself are interesting: when the effect of depolarization is taken into account and the condition

$$1-\alpha\Pi(\omega_G) = 0 \tag{19}$$

can be satisfied for real ω_G, the spectral dependencies of σ_{yy} and $\chi_\perp$ must be substantially modified in the spectral region $\omega \approx \omega_G$. It is clear that (19) can be satisfied only if $\mathrm{Im}\,\Pi(\omega_G) = 0$ and the possibility of satisfying (19) is essentially related to the properties of $\Pi(\omega)$.

In this section we will calculate $\Pi(\omega)$ and conditions for the appearance of a solution of (19) in the collisionless approximation. From (17) we have

$$\begin{aligned}\mathrm{Im}\,\Pi(\omega) = \frac{2e^2(T/\hbar)^2\,\Delta z}{\epsilon v_H^2\hbar\omega}&\{[2\varepsilon_H\varepsilon_F+T^2-(\hbar\omega/2)^2-\varepsilon_H\hbar\omega]^{1/2}\\ &-[2\varepsilon_H\varepsilon_F+T^2-(\hbar\omega/2)^2+\varepsilon_H\hbar\omega]^{1/2}\}[(\hbar\omega/2)^2-T^2]^{-1/2}\end{aligned} \tag{20}$$

and $\mathrm{Im}\,\Pi(\omega)$ is finite in the region $2T/\hbar < \omega < \omega_m$; here $\hbar\omega_m/2 = \varepsilon_H + (T^2+\varepsilon_H^2+2\varepsilon_H\varepsilon_F)^{1/2} > T$ and, hence, $\omega_m \to 2T$ for $H \to 0$. Using the Kramers–Kronig relation, we can express the real part of $\Pi(\omega)$ as

$$\mathrm{Re}\,\Pi(\omega) = \frac{2}{\pi}\int_0^\infty \mathrm{d}\xi\;\frac{\xi\,\mathrm{Im}\,\Pi(\xi)}{\xi^2-\omega^2}. \tag{21}$$

Since $\mathrm{Im}\,\Pi(\omega) \leqslant 0$, it then follows that $\mathrm{Re}\,\Pi(\omega) < 0$ for $\omega < 2T/\hbar$ and $\mathrm{Re}\,\Pi(\omega) > 0$ for $\omega > \omega_m$. In addition, for $\omega > \omega_m$ the function $\mathrm{Re}\,\Pi(\omega)$ goes monotonically to zero with increasing ω. Hence, equation (19) has an only root, in the region where $\omega > \omega_m$,

if $\alpha\Pi(\omega_m) > 1$. At $\omega = \omega_m$, assuming that the magnetic field is not too strong, so that $2\varepsilon_H/T \ll 1$, we obtain

$$\alpha\Pi(\omega_m) \approx \alpha(\Delta z/a_B)(T/2\varepsilon_H) \tag{22}$$

where a_B is the effective Bohr radius. To be specific we will consider numerically two DQWs based on GaAs/Al_xGa_{1-x}As with parameters: $T = 2.6$ meV, $n = 2.5 \times 10^{11}$ cm^{-2} (case I) and $T = 1.3$ meV, $n = 1.25 \times 10^{11}$ cm^{-2} (case II); for both DQWs it is assumed that $\Delta z = 130$ Å, $\alpha \approx 0.84$ and $\Delta = \delta_H = 0$. We notice that for the model of flat-band symmetric DQWs the conditions stated above can be satisfied if $d = 100$ Å, $d_b = 30$ Å, and $x = 0.38$ ($x = 0.55$) for case I (II). Below, we denote these DQWs as I-DQWs and II-DQWs. Then from (22), $\alpha\Pi(\omega_m) \approx 1.1(T/2\varepsilon_H) \gg 1$, i.e., equation (19) should be satisfied. As follows from (19) and (22), the appearance of the root ω_G is possible in DQW systems under rather strong H, provided that the ratio $\Delta z/a_B$ and the tunnelling matrix element T are not too small.

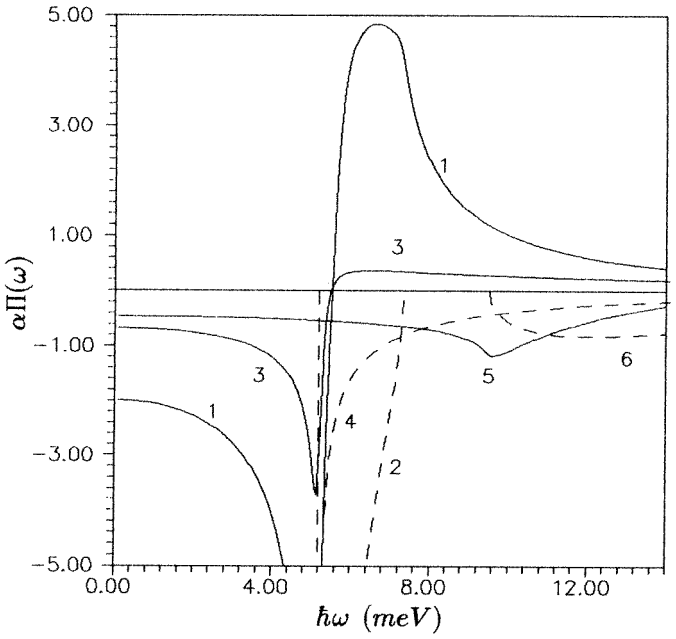

Figure 1. Energy dependencies of the collisionless response function in I-DQWs for the cases: (i) $H = 2$ T, curves 1 and 2; (ii) $H = 8$ T, curves 3 and 4; and (iii) $H = 12$ T, curves 5 and 6. The solid curves 1, 3 and 5 show $\alpha\,\mathrm{Re}\,\Pi(\omega)$ and $10\,\alpha\,\mathrm{Re}\,\Pi(\omega)$, respectively. The dashed curves 2, 4 and 6 show $\alpha\,\mathrm{Im}\,\Pi(\omega)$ and $10\,\alpha\,\mathrm{Im}\,\Pi(\omega)$, respectively. For curve 1 the minimum is close to -14.5.

The case of I-DQWs is illustrated in figure 1, where we plot $\mathrm{Im}\,\Pi(\omega)$ given by (20), and $\mathrm{Re}\,\Pi(\omega)$ as functions of ω for the cases: (i) at $H = 2$ T, curves 1 and 2; (ii) at $H = 8$ T, curves 3 and 4; and (iii) at $H = 12$ T, curves 5 and 6. Solid curves 1 and 3 show $\alpha\,\mathrm{Re}\,\Pi(\omega)$, and solid curve 5 shows $10\,\alpha\,\mathrm{Re}\,\Pi(\omega)$. Dashed curves 2 and 4 demonstrate $\alpha\,\mathrm{Im}\,\Pi(\omega)$, and dashed curve 6 shows $10\,\alpha\,\mathrm{Im}\,\Pi(\omega)$. The behaviour of the energy spectra for cases (i)–(iii) is discussed in section 1. In figure 2 we plot the same dependencies (e.g., curve 2 in figure 1 and curve 2 in figure 2 correspond to $\alpha\,\mathrm{Im}\,\Pi(\omega)$ for case (ii), for which the Fermi level intersects the anticrossing gap and only the lowest of the tunnel-coupled

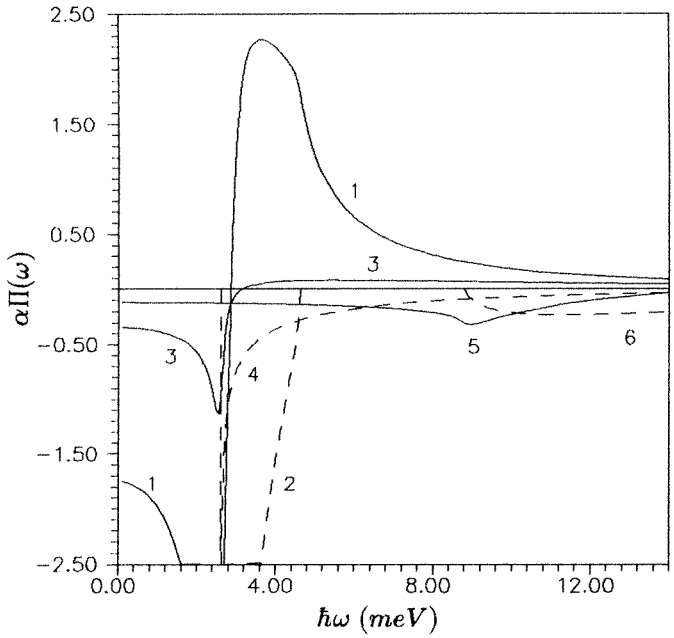

Figure 2. As figure 1, but for II-DQWs (see the parameters in the text) for cases (i), (ii) and (iii), $H = 2$ T, 7 T and 10 T, respectively. Other parameters and notation are the same as those for figure 1. For curve 1 the minimum is close to -7.5.

levels is occupied) for the II-DQWs; here $H = 2$ T, 7 T, and 10 T for the cases (i), (ii), and (iii), respectively. From figures 1 and 2 it follows, consistently with our analytical consideration, that only for $H = 2$ T, for which both tunnel-coupled levels are occupied, is it possible to satisfy equation (19), while stronger H suppresses this possibility. In addition (see also (22)), since the value of $(T/2\varepsilon_H)$ for case (i) in figure 2 is two times smaller than in figure 1, $\alpha\Pi(\omega_m)$ (> 1) in figure 2 is also approximately two times smaller than in figure 1. Notice that the behaviour of the curves 1 and 3 in the lower half-plane is qualitatively similar (in figure 1 and in figure 2); for curves 1 in figures 1 and 2 the minimum values are approximately equal to -14.5 and -7.5, respectively. In correspondence with the above remarks (see also below), the groups of curves (2, 4, 6) and (1, 3, 5) in figures 1 and 2 demonstrate also, in arbitrary units, the absorption and the phase shift in the Voigt effect, respectively (without the effect of depolarization). Because of the contribution of virtual intersubband transitions (appearing due to modification of the selection rules), an increase of the Voigt effect takes place near the lower absorption edge $\hbar\omega < 2T$, if the effect of depolarization is neglected. In the next section we will show that this increase vanishes completely when the effect of depolarization is taken into account.

4. Spectral dependencies of responses

In this section we will take into account the effect of the depolarization. In our numerical study we will treat, besides the collisionless approximation, the case of the finite broadening energy $2\Gamma = 0.2$ meV, which makes it possible to estimate the smoothing of the spectral peculiarities due to collisions (notice that this value of Γ corresponds to a mobility

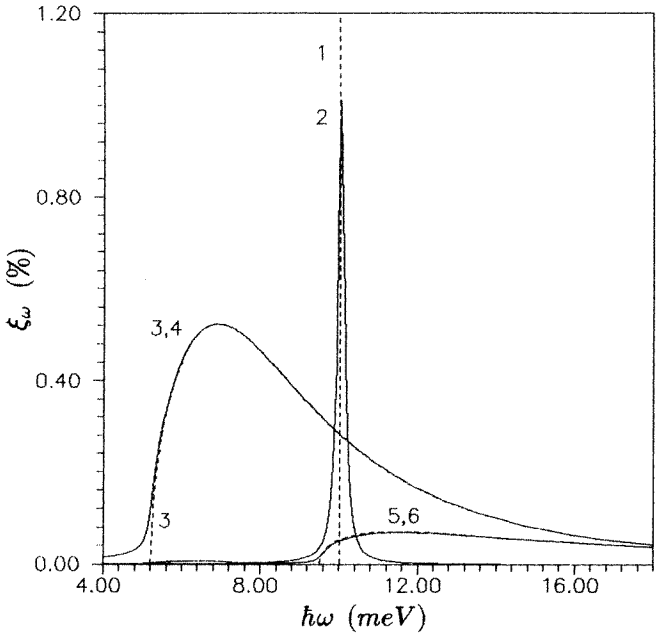

Figure 3. Energy dependencies of the absorption ξ_ω (in per cent) for I-DQWs and magnetic fields, in cases (i)–(iii), as for figure 1. In figures 3–8: dashed curves (1, 3, 5) correspond to the collisionless approximation; solid curves (2, 4, 6) correspond to the finite level broadening $2\Gamma = 0.2$ meV. Curve 1 at $\overline{h}\omega \approx 10$ meV represents δ-function behaviour.

approximately equal to 8.5×10^4 cm^2 V^{-1} s^{-1}, which is rather small for the GaAs-based DQWs). In this section, dashed (solid) curves 1, 3, 5 (2, 4, 6) in figures 3–8 plot the results obtained in the collisionless approximation (for the finite Γ).

4.1. Absorption

It is appropriate [15] to introduce a dimensionless value $\xi_\omega = 2\,\mathrm{Re}(\boldsymbol{E}\hat{\sigma}(\omega)\boldsymbol{E})/S$ which is determined by the ratio of the power absorption in the DQWs to the Poynting vector $S = (c\sqrt{\epsilon}/2\pi)|\boldsymbol{E}|^2$ for the external field. Only the E_y-component of the electric field contributes in the power absorption in the DQWs. For $\boldsymbol{E} \parallel 0Y$, we have

$$\xi_\omega = \frac{4\pi}{c\sqrt{\epsilon}}\,\mathrm{Re}\,\sigma_{yy}(\omega). \tag{23}$$

From (15) and (23) it follows that $\xi_\omega \neq 0$ only in the region where $\mathrm{Im}\,\Pi(\omega) \neq 0$, if $\omega \neq \omega_G$. However, in the collisionless approximation, at $\omega \approx \omega_G$ we have a delta-function form of ξ_ω, i.e., the resonant enhancement of absorption at ω_G. For finite Γ this peak acquires finite width and height.

In figure 3 we plot ξ_ω for I-DQWs and magnetic fields, corresponding to cases (i)–(iii), as for figure 1. Comparing figure 3 with the curves in figure 1 that represent ξ_ω in the absence of the depolarization effect, we can see that in cases (i) and (ii), for $H = 2$ T and $H = 8$ T, this effect removes the square-root divergence at $\overline{h}\omega \to 2T$. In addition, it strongly suppresses absorption within the region $2T/\overline{h} < \omega < \omega_m$ in case (i). However, it slightly changes the absorption in the main part of the absorption region for case (ii).

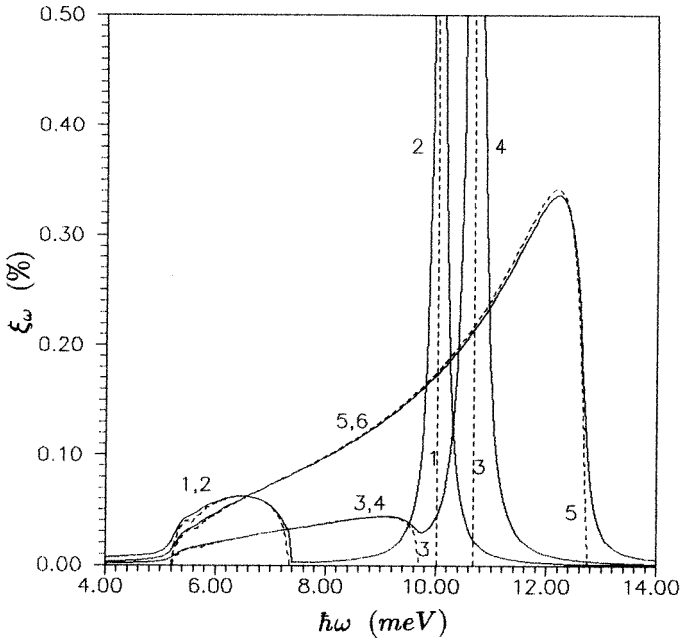

Figure 4. Energy dependencies of the absorption for I-DQWs in case (i): $H = 2$ T for curves 1 and 2; $H = 3$ T for curves 3 and 4; and $H = 4$ T for curves 5 and 6. Curve 1 and the part of curve 2 for $\bar{h}\omega \leqslant 7.35$ meV represent $10\,\xi_\omega$.

Similar changes are small over the whole of the absorption region for case (iii). Curve 1 at $\bar{h}\omega = \bar{h}\omega_G \approx 10$ meV represents the delta-function behaviour of ξ_ω. At finite Γ, this peak, as is seen from curve 2, has a finite width and height but still shows a substantial resonant enhancement of absorption at $\omega \approx \omega_G$.

In figure 4, for I-DQWs and magnetic fields corresponding only to case (i) ($H = 2$ T for curves 1 and 2, $H = 3$ T for curves 3 and 4, $H = 4$ T for curves 5 and 6), ξ_ω is plotted as the curves 3–6 and with the part of curve 2 for $\bar{h}\omega > 7.35$ meV. Curve 1 and the part of curve 2 for $\bar{h}\omega \leqslant 7.35$ meV show $10\,\xi_\omega$. Notice that for $\omega_m > \omega > 2T/\bar{h}$, curves 1 and 2 practically coincide: here $\bar{h}\omega_m \approx 7.35$ meV. The maxima of curves 2 and 4 are close to 1.0 and 1.3, respectively. The curves in figure 4 demonstrate that with increasing H, the frequency (and the amplitude) of the resonance absorption ω_G increases before the disappearance of this resonance. As $H \to 0$ the amplitude (i.e., the integral strength) of the resonance absorption at ω_G will go to zero as H^2; here $\omega_G/2T \to (1 + 2\alpha\,\Delta z/a_B)^{1/2}$. From figure 4 (in the collisionless approximation) it follows that the upper boundary, ω_m, of the lower absorption peak quickly increases with increasing H. At the same time, the position of the δ-function absorption peak, ω_G, increases much more slowly. Therefore, for sufficiently large H the two peaks overlap. As a result, the spectral dependence of the absorption becomes smooth for all frequencies.

For the II-DQWs and magnetic fields, in cases (i)–(iii), as for figure 2, in figure 5 we plot ξ_ω as curves 1–4 and $10\,\xi_\omega$ as curves 5 and 6. Comparing these dependencies with the curves in figure 2 (which represent ξ_ω in the absence of the depolarization effect), we can see that in cases (i) and (ii), for $H = 2$ T and $H = 7$ T, this effect removes the square-root divergence for $\bar{h}\omega \to 2T$. In addition, it strongly suppresses absorption within

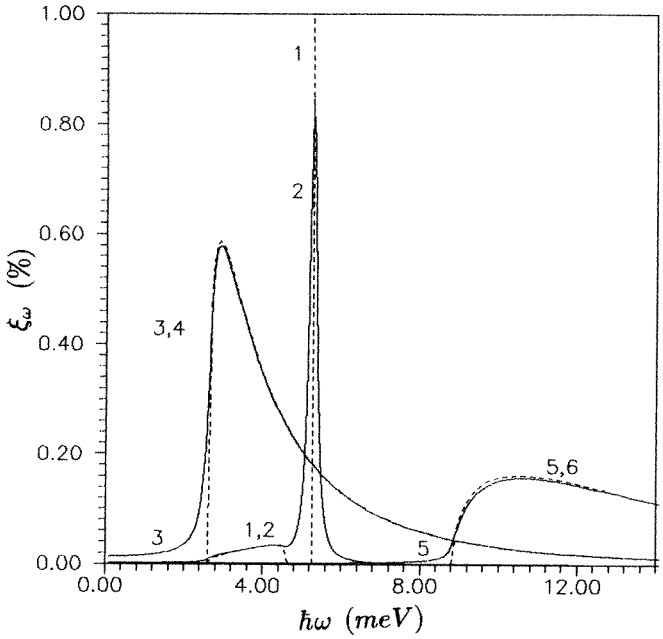

Figure 5. Energy dependencies of the absorption for II-DQWs and magnetic fields corresponding to cases (i)–(iii), as in figure 2. Curves 5 and 6 show $10\,\xi_\omega$. Curve 1 at $\overline{h}\omega \approx 5.2$ meV represents δ-function behaviour.

the main part of the region $2T/\overline{h} < \omega < \omega_m$ in case (i) (here $\overline{h}\omega_m \approx 4.6$ meV). However, it only slightly changes the absorption in the main part of the absorption region for case (ii). Similar changes are very small over the whole absorption region for case (iii). In all three cases, (i)–(iii), the relative change due to the depolarization is substantially smaller in DQWs with smaller n and T, as follows from a comparison of figures 3 and 5 with figures 1 and 2. Curve 1 at $\overline{h}\omega = \overline{h}\omega_G \approx 5.2$ meV represents delta-function behaviour of ξ_ω. At a finite Γ, this peak, as is seen from the curve 2, has some finite width and height but still shows a substantial resonant enhancement of the absorption at $\omega \approx \omega_G$.

The absorption caused by the E_z-component (perpendicular to the DQW planes) can be described in a similar way. Effective components of the conductivity are related as $\sigma_{zz}(\omega) = (\omega/\omega_c)^2[\sigma_{yy}(\omega) - \sigma_{xx}(\omega)]$. As in [12], it appears that the ratio $\mathrm{Re}\,\sigma_{zz}(\omega)/\mathrm{Re}\,\sigma_{yy}(\omega)$ is equal to $(\omega/\omega_c)^2$. Therefore, the spectral dependencies of the absorption in this case can be deduced from the dependencies represented above with their multiplication by the factor $(\omega/\omega_c)^2$.

4.2. The Voigt effect

Transformation of the linearly polarized high-frequency wave to the elliptically polarized wave (the Voigt effect) can be characterized [16] by the phase shift $\delta_\omega = \mathrm{Im}(E'_y/E'_x)_{E_x=E_y}$, where $\boldsymbol{E}'$ is the total electric field transmitted through the DQWs. This expression for δ_ω is valid when $|\delta_\omega| \ll 1$. Then we have

$$\delta_\omega \approx \frac{2\pi}{c\sqrt{\epsilon}}\,\mathrm{Im}\,[\sigma_{xx}(\omega) - \sigma_{yy}(\omega)] = \frac{4\pi\, v_H}{c\sqrt{\epsilon}}\,\mathrm{Im}\,[\chi_\perp(\omega)]. \tag{24}$$

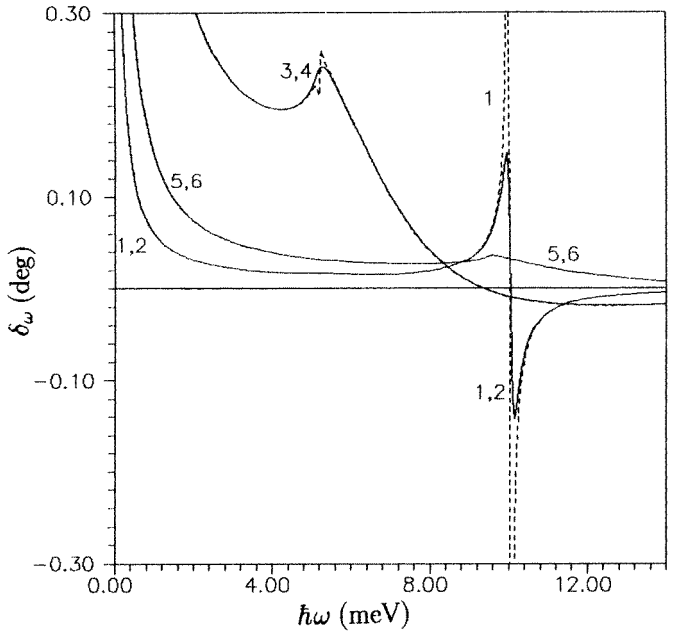

Figure 6. Energy dependencies of the phase shift δ_ω (in degrees) in I-DQWs for the cases: (i) $H = 2$ T, curves 1 and 2; (ii) $H = 8$ T, curves 3 and 4; and (iii) $H = 12$ T, curves 5 and 6. Curves 5 and 6 practically coincide.

In figure 6 we plot δ_ω (in degrees) for I-DQWs and the same magnetic fields (cases (i)–(iii)) as in figures 1 and 3. Near $\hbar\omega_G \approx 10$ meV, the dependence of the phase shift δ_ω of ω is determined by a contribution of the virtual transitions which correspond to resonance absorption at the frequency ω_G, so $|\delta_\omega|$ is strongly enhanced in case (i).

In figure 7 we plot δ_ω for I-DQWs and the same magnetic fields as in figure 4, i.e., only for case (i) ($H = 2$ T for curves 1 and 2, $H = 3$ T for curves 3 and 4, and $H = 4$ T for curves 5 and 6). The solid curves in figure 7 demonstrate that with increasing H, the maximum modulus of δ_ω near the resonance frequency ω_G considerably increases before the disappearance of the resonance behaviour at sufficiently high H.

In figure 8 we plot δ_ω for II-DQWs and the same magnetic fields (cases (i)–(iii)) as in figures 2 and 5.

We notice that in case (i) in figures 6–8 the solid and dashed curves have substantial differences only for $\omega \approx \omega_G$. In case (iii) in figures 6–8 the solid and dashed curves practically coincide for all ω. For case (ii) in figures 6 and 8 the solid and dashed curves are clearly different in the vicinity of $\omega = 2T/\hbar$. So at this frequency the derivative of curve 3 goes to ∞ (i.e., in the collisionless approximation). However, δ_ω is finite. Such a behaviour is determined by the δ_ω-dependence versus $\Pi(\omega)$ and also by the smooth dependence of $\mathrm{Re}\,\Pi(\omega)$ and sharp increase of $|\mathrm{Im}\,\Pi(\omega)|$ near to $\omega = 2T/\hbar$ (see equations (15) and (24)). It is clear that this jump of δ_ω at $\omega = 2T/\hbar$ should be smaller for larger $|\mathrm{Re}\,\Pi(\omega)|$. Then, from curves 3 in figures 1 and 2 we conclude that the jump should be stronger in figure 8 than in figure 6. Indeed, it is in agreement with the behaviour shown by curves 3 in figures 6 and 8.

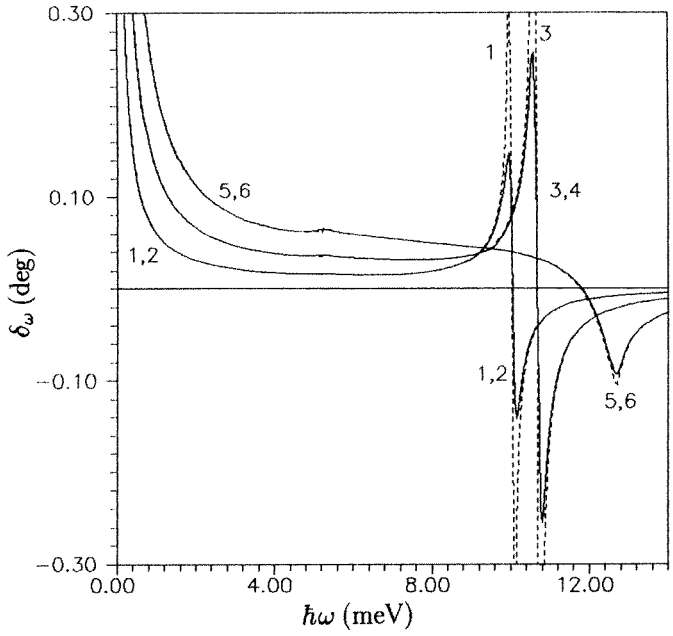

Figure 7. Energy dependencies of the phase shift in I-DQWs for case (i): $H = 2$ T, curves 1 and 2; $H = 3$ T, curves 3 and 4; and $H = 4$ T, curves 5 and 6.

4.3. The transverse dipole moment

From (24) it follows that δ_ω is proportional to the imaginary part of the longitudinal–transversal susceptibility. In the collisionless approximation, for a transparency region, $\mathrm{Re}\,\chi_\perp(\omega) \equiv 0$ as follows from (16) and the properties of $\Pi(\omega)$, if $\omega \neq \omega_G$. Hence, for such a transparency region, treating δ_ω, we also study the transverse dipole moment, or $\chi_\perp(\omega)$. In addition, for the region where the absorption takes place (and also when the level broadening is taken into account) we have $\mathrm{Re}\,\chi_\perp(\omega) = -(c\sqrt{\epsilon}/4\pi\omega_c\,\Delta z)\xi_\omega$. Therefore, in any region, calculation of δ_ω and ξ_ω gives us also $\mathrm{Im}\,\chi_\perp(\omega)$ and $\mathrm{Re}\,\chi_\perp(\omega)$, respectively. Because of possible implications of the excitation of the transverse dipole moment by an in-plane electric field, it is interesting to estimate the value of the dimensionless longitudinal–transversal susceptibility. In figure 9 we plot $\mathrm{Re}\,\chi_\perp(\omega)$ (dashed curves 1 and 3) and $\mathrm{Im}\,\chi_\perp(\omega)$ (solid curves 2, 4 and 6) for I-DQWs and the same magnetic fields (cases (i)–(iii)) as in figure 6. The dashed curve 5 corresponds to $10\,\mathrm{Re}\,\chi_\perp(\omega)$. Near to $\hbar\omega_G \approx 10$ meV, $\chi_\perp(\omega)$ as a function of ω (curves 1 and 2 at $H = 2$ T) represents strong resonance behaviour and its modulus can be about 12.5. The collisional broadening is taken into account for all of the curves in figure 9.

5. Conclusion

In this article we have demonstrated peculiarities of the high-frequency response of electrons in DQWs under an in-plane magnetic field. The frequencies, depending on the value of the in-plane magnetic field and the DQW parameters, for which the peculiarities pointed out can be observed, belong to the submillimetre region. Hence, experimental

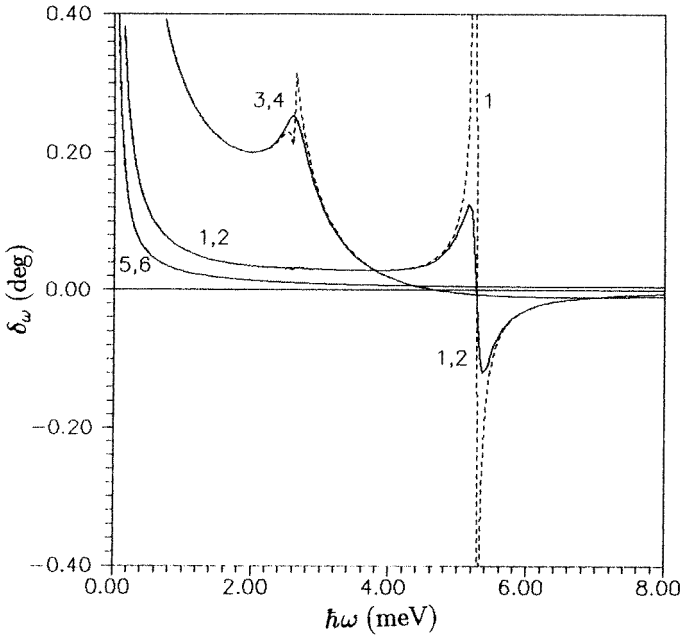

Figure 8. Energy dependencies of the phase shift in II-DQWs for the cases: (i) $H = 2$ T, curves 1 and 2; (ii) $H = 7$ T, curves 3 and 4; and (iii) $H = 10$ T, curves 5 and 6. Curves 5 and 6 practically coincide.

observations are possible using both a standard technique for this spectral region and new experimental methods (emission of a free-electron laser [17, 18] and transitional time-domain spectroscopy of the emission under an ultrafast excitation of the heterostructure [19]), developed recently for the THz region. As represented in section 4, numerical estimates demonstrate the possibility of absorption and Voigt effect measurements in these spectral regions. In addition, *transformation* of the y-component of the electric field into oscillations of the dipole moment perpendicular to the DQWs, determined by the susceptibility $\chi_\perp$, appears to be sufficiently effective.

Let us list the assumptions which have been made in our calculations. We have assumed that an in-plane magnetic field is sufficiently low that the approximation of 'rigid' (i.e., independent of Δ and ω_c) orbitals is valid. It can be shown that further contributions due to the magnetic field to the electron spectra and eigenfunctions of the DQWs are negligible when the dimensionless parameter $A_H(d/\pi\ell_H)^4$ is small in comparison with unity (here ℓ_H is the magnetic length and $A_H \sim 1$). For the strongest magnetic field considered above, $H = 12$ T, we estimate this parameter as 0.016 for the flat-band DQWs with $d = 100$ Å. Hence, even in this case our approximation is well justified. We have used a collisionless approximation or a simple assumption which implies a finite collisional broadening of peaks. Moreover, the dependencies of Γ on Δ and the magnetic field are assumed to be weak. The random-phase approximation has been used: for the static case Δ is assumed to be a parameter controlled by the transverse voltage applied to the DQWs, while the high-frequency response is considered without taking into account the exchange and correlation contributions. The two-level tunnel approximation has been used, and T is assumed to be independent of H. Finally, we have used a simple electron band structure without

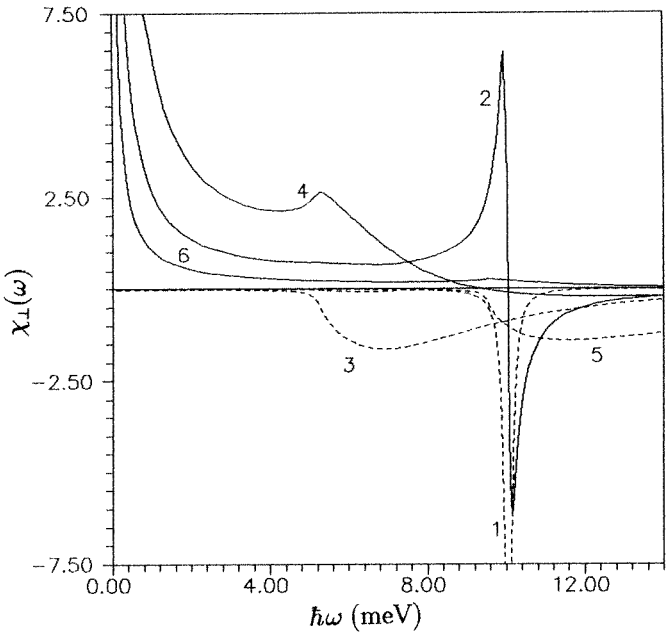

Figure 9. Energy dependencies of the longitudinal–transversal susceptibility in I-DQWs for the cases: (i) $H = 2$ T, curves 1 and 2; (ii) $H = 8$ T, curves 3 and 4; and (iii) $H = 12$ T, curves 5 and 6. The dashed curves 1 and 3 show $\mathrm{Re}[\chi_\perp(\omega)]$. The solid curves (2, 4, and 6) show $\mathrm{Im}[\chi_\perp(\omega)]$. The dashed curve 5 corresponds to $10\,\mathrm{Re}\,[\chi_\perp(\omega)]$. All of the curves correspond to $2\Gamma = 0.2$ meV.

nonparabolicity, or contributions of Γ and X valleys, which has already been discussed in the literature. None of these approximations change either the qualitative behaviour of the dependencies considered or the numerical estimates given here.

In conclusion, the shapes of the spectral dependencies of the absorption and the Voigt effect due to intersubband transitions of electrons in the DQWs under an in-plane magnetic field are determined by the peculiarities of the dispersion laws of this system. Hence, their direct measurement in the submillimetre (THz) spectral regions can provide a straightforward method for investigation of such peculiarities. It is found that the depolarization effect substantially modifies these spectral dependencies. It is shown that the Voigt effect and the transverse dipole moment can be resonantly enhanced in the high-frequency transparency region ($\omega > \omega_m$). In addition, we have demonstrated the possibility of transformation of the normally incident wave into transverse (to the DQW plane) dipole oscillations.

Acknowledgment

The research described in this publication was made possible in part by Grant U65000 from the International Science Foundation.

References

[1] Eisenstein J P 1992 *Superlatt. Microstuct.* **12** 107
[2] Huang Y and Lien C 1995 *Phys. Low-Dim. Struct.* **4/5** 1

[3] Lyo S K 1994 *Phys. Rev.* B **50** 4965
[4] Simmons J A, Lyo S K, Harff N E and Klem J F 1994 *Phys. Rev. Lett.* **73** 2256
[5] Kurobe A, Castleton I M, Linfield E H, Grimshaw M P, Brown K M, Ritchie D A, Pepper M and Jones G A C 1994 *Phys. Rev.* B **50** 4889
[6] Ohno Y, Sakaki H and Tsuchiya M 1994 *Phys. Rev.* B **49** 11 492
[7] Berk Y, Kamenev A, Palevski A, Pfeiffer L N and West K W 1995 *Phys. Rev.* B **51** 2604
[8] Salvador A, Teraguchi W, Reed J and Morkoc H 1992 *Phys. Rev.* B **46** 12 757
Reynolds D C, Evans K R, Jogai B, Stutz C E and Yu P W 1993 *Solid State Commun.* **86** 339
[9] Heberly A P, Oestreich M, Haacke S, Ruhle W W, Maan J C and Kohler K 1994 *Phys. Rev. Lett.* **72** 1522
[10] Ando T, Fowler A B and Stern F 1982 *Rev. Mod. Phys.* **54** 437
[11] Ando T 1979 *Phys. Rev.* B **19** 2106
[12] Dempsey J and Halperin B I 1993 *Phys. Rev.* B **47** 4662, 4674
[13] Vasko F T and Raichev O E 1995 *Zh. Eksp. Teor. Fiz.* **107** 951 (Engl. Transl. 1995 *Sov. Phys.–JETP* **80** 539)
[14] Zaluzny M 1994 *Appl. Phys. Lett.* **65** 1817
[15] Vasko F T 1993 *Electron States and Optical Transitions in Semiconductor Heterostructures* (Kiev: Naukova Dumka)
[16] Landau L D and Lifshitz E M 1960 *Electrodynamics of Continuous Media* (Oxford: Pergamon)
[17] Keay B J, Guimaraes P S S, Kaminski J P, Allen S J Jr, Hopkins P F, Gossard A C, Florez L T and Harbison J P 1994 *Surf. Sci.* **305** 385
[18] Scott J S, Kaminski J P, Allen S J, Chow D H, Lui M and Liu T Y 1994 *Surf. Sci.* **305** 389
[19] Katzenellenbogen N and Grischkowsky D 1992 *Appl. Phys. Lett.* **61** 840